ACES Asian Chemical Editorial Society

DOI: 10.1002/asia.201601403

CHEMISTRY AN ASIAN JOURNAL Full Paper

Helical Structures

Superhelices Self-Assembled from Polypeptide-Based Polymer Mixtures: Multistranded Features

Xingyu Zhu, Jiaping Lin,* and Chunhua Cai*[a]

Abstract: Poly(γ-benzyl-L-glutamate)-block-poly(ethylene glycol) (PBLG-*b*-PEG) rod–coil block copolymers and poly(γ-benzyl-L-glutamate) (PBLG) homopolymers can cooperatively self-assemble into superhelical structures in aqueous solution. Herein, we discovered that the helices can have multiple strands with tunable characteristics. The strand number was dependent on the initial polymer concentration of the self-assembly, the self-assembly temperature, and the weight fraction of the block copolymers in the mixture. Higher initial polymer concentrations or lower weight fractions of the block copolymers induced the formation of helices with larger diameters and higher strand numbers, and helices prepared at higher temperatures had higher strand numbers. Based on an analysis of the correlation between the geometric parameters of the helices and the strand number, a possible mechanism for the formation of multistranded superhelices is suggested.

Introduction

Helical structures exist widely in natural biological systems.[1] For example, the tobacco mosaic virus has a core–shell superhelical structure with RNA as the core and helically warped coating proteins as the shell.[2] The strand number is one of the basic features of a helical structure. In addition to single helices, multistranded helices are also observed. DNA, the fundamental material of life, consists of two nucleic acid strands that are twisted into a double helix.[3] Triple-stranded nucleic acid helices are also observed under certain conditions.[4] Collagen is a type of triple-stranded helix that is generated by three protein chains screwed together.[5] Inspired by these biological helical structures in nature, researchers have paid considerable attention to self-assembled superhelical structures in solution because of their potential applications in bionics and advanced functional materials.[6]

Ho et al. reported that poly(styrene)-*b*-poly(L-lactide) (PS-PLLA) block copolymers self-assemble into helical structures through scrolling of the polymer ribbons.[6c] Novak et al. prepared superhelical structures from mixtures of a polycarbodiimide-*b*-PEG (PEG = poly(ethylene glycol)) block copolymer and polycarbodiimide homopolymer.[6d,7] In their work, superhelices with defined chirality were formed when the rod blocks and rod homopolymers in the mixtures possessed the same chirality. In several reports, superhelical structures with multistranded features were obtained.[8] For example, through the coassembly of poly(acrylic acid)-block-poly(methyl acrylate)-block-polystyrene (PAA-*b*-PMA-*b*-PS) triblock copolymers with different multiamines, Pochan and co-workers prepared a mixture of single and double superhelices.[8b] The double helices were composed of two individual helical cylinders with a pitch that was twice that of the single helices. Liu et al. discovered that poly(*n*-butyl methacrylate)-block-poly(2-cinnamoyloxyethyl methacrylate)-block-poly(*tert*-butyl acrylate) (PBMA-*b*-PCEMA-*b*-PtBA) triblock copolymers can self-assemble into both double and triple helices.[8a] However, in these reports, the formation mechanism of the multistranded superhelices was not fully discussed. Specifically, the significant factors that induced the formation of helices with various strand numbers were not revealed, and the strand number of the superhelices was not controllable.

In previous works, we obtained superhelical structures through the coassembly of poly(γ-benzyl-L-glutamate)-block-poly(ethylene glycol) (PBLG-*b*-PEG) block copolymers and poly(γ-benzyl-L-glutamate) (PBLG) homopolymers.[9] With the assistance of simulations, it was found that the homopolymers formed a rigid bundle and the rod–coil block copolymers screwed onto the bundle to form a helical shell.[10] The chirality of the helices can be tuned by the self-assembly temperature and initial solvent nature.[11] The ordered packing of the rigid PBLG blocks of the copolymer is believed to be significant for the formation of structures, and the packing mode of the pendant phenyl groups of the PBLG side chains is responsible for the superhelical chirality. In addition to the superhelical chirality, the strand number is another important characteristic

[a] X. Zhu, Prof. Dr. J. Lin, Dr. C. Cai
Shanghai Key Laboratory of Advanced Polymeric Materials
State Key Laboratory of Bioreactor Engineering
Key Laboratory for Ultrafine Materials of Ministry of Education
School of Materials Science and Engineering
East China University of Science and Technology
NO.130 Meilong road, Shanghai 200237 (China)
E-mail: jlin@ecust.edu.cn
caichunhua@ecust.edu.cn

Supporting information for this article can be found under: http://dx.doi.org/10.1002/asia.201601403.

of helical structures. Although polymeric supramolecular helices have been reported in several cases,[12] the mechanism behind the control of the strand number of a multistranded superhelix has not been fully explored.[13] Herein, we extend our previous work to explore the multistranded features of superhelical structures formed by self-assembly of the polypeptide-based polymer mixture system.

Herein, we discovered that PBLG-*b*-PEG/PBLG mixtures can self-assemble into multistranded superhelices. The strand number of the superhelices was found to be dependent on certain parameters, such as the initial polymer concentration, self-assembly temperature, and molecular weight of the block copolymers in the polymer mixtures. Based on the analysis of the relationship between the geometric parameters in the helical structure (diameter, helical angle, pitch, and strand number) and the experimental factors, a possible mechanism was proposed to illustrate how these factors control the self-assembled superhelical structures.

Results and Discussion

Multistranded Superhelical Structures

PBLG-*b*-PEG block copolymers and PBLG homopolymers can cooperatively self-assemble into superhelical structures. In the self-assemblies, the homopolymers form a rigid bundle and the rod–coil block copolymers screw onto the bundle to form a helical shell.[9b,10b] Without the homopolymers, the PBLG-*b*-PEG block copolymers self-assemble into uniform spheres approximately 250 nm in diameter (Figure S1). Figure 1a shows a typical SEM image of the superhelical structures self-assembled from the PBLG-*b*-PEG/PBLG polymer mixture. The initial solvent was THF/DMF (3:7 v/v) and the initial polymer concentration was 0.5 g L^{-1}. The superhelices have left-handed chirality (CD spectra for the superhelices can be found in Figure S2 in the Supporting Information), and the pitch of the screwed structure is almost uniform. Careful examination of the strands on the helices revealed that some of the self-assembled structures have the characteristics of double or triple helices. Figure 1b shows the magnified image of the superhelix indicated in the red square in Figure 1a. The strands of the helix are marked by dotted curves, which reveal the triple-helical structure. A multistranded structure with a different strand number can be observed in one helical aggregate. As shown in Figure 1c (magnified image of the helical structure marked by the green square in Figure 1a), a dislocation appears at the point at which the helix transforms from double strand to triple strand (details of the dislocations are discussed below). To further confirm the multistranded feature of the helices, a cross-sectional image of ultramicrotomed superhelices was characterized by using TEM. Figure 1d, insets, shows schematic illustrations of cross sections of single (blue lines) and double (red lines) helical structures. As shown in Figure 1d, the cross section of the single helix shows a feature of one strand (blue circle), whereas the cross section of the double helix shows a feature of two strands (red circle). The observed structures match well with the cross section of superhelices with multiple strands. Moreover, the cross section of the helices is shown in the contrast-enhanced TEM image (Figure S3). The existence of superhelical structures with multiple strands was further verified by a microtome section under TEM.

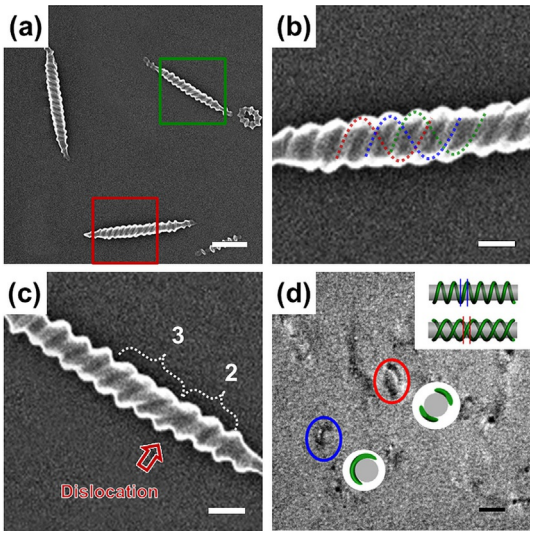

Figure 1. a) SEM images of helical aggregates self-assembled from $PBLG_{20000}$-*b*-PEG_{5000}/$PBLG_{528000}$. b, c) Magnified images of the helical structures marked by b) a red square and c) a green square in a). The numbers in the images represent the strand number of the helical structures. d) TEM cross-sectional image of ultramicrotomed superhelices. Top-right inset: Illustrations of a single and double helix that correspond to the blue and red circles. The self-assemblies were prepared at 50 °C. The initial polymer concentration was 0.5 g L^{-1} and the weight fraction of PBLG-*b*-PEG ($f_{PBLG\text{-}b\text{-}PEG}$) in the polymer mixture was 0.8. Scale bars: 400 (a), 100 (b and c), and 200 nm (d).

Figure 2 compares images of single and double helices, from which the difference in strand number between the helices can be determined. The basic feature of a helix is that the tangent line at any point of the strand makes a constant angle (helical angle α) with the central axis of the helix.[14] Based on this feature, we determined the number of strands in the helix from the SEM images (Figures 2a and e). The strand number of the helices was further confirmed by comparing the TEM, AFM, and cryo-TEM images of single and double helices. As revealed by the TEM images, the helical angle is about 70.8° for the single helix in Figure 2b and around 61.9° for the double helix in Figure 2f. From the three-dimensional AFM images (Figures 2c and g), we determined the difference between these two types of helices, that is, the double helix has a larger helical angle. Moreover, note that the pitches of the single and double helices are almost equal (≈73 nm). As shown in the cryo-TEM images (Figures 2d and h), the single and double helices have different characteristics and the double helix consists of two strands with the same axis. Cryo-TEM images confirmed that the multistranded helices existed in solution and ruled out changes in morphology during the drying process.

To deepen our understanding of the formation mechanism of multistranded helical structures, we further examined the variation in the structural parameters of superhelices as a function of the initial polymer concentration (C), the self-assembly temperature (T), and the weight fraction of the PBLG-*b*-PEG block copolymer ($f_{PBLG\text{-}b\text{-}PEG}$) in the polymer mixtures. Figure 3a–

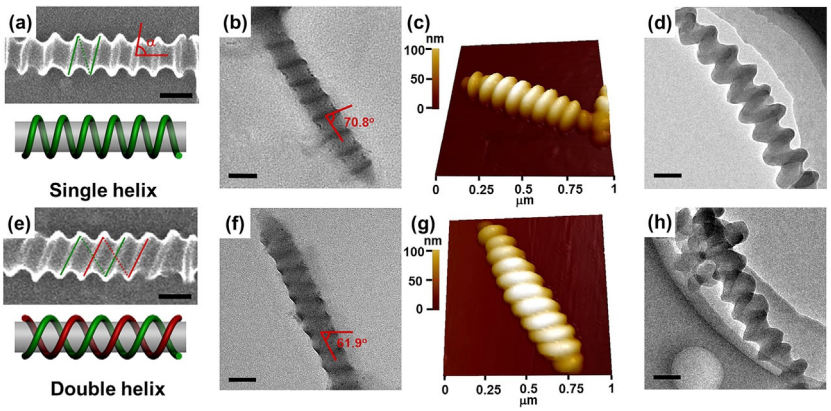

Figure 2. Comparison of a)–d) single and e)–h) double helices: a, e) SEM; b, f) TEM; c, g) AFM; and d, h) cryo-TEM images of helical aggregates self-assembled from $PBLG_{20\,000}$-*b*-PEG_{5000}/$PBLG_{528\,000}$. a, e) Illustrations of single and double helices, respectively, are also shown. The self-assemblies were prepared at 50 °C. The initial polymer concentration was 0.5 g L^{-1} and the weight fraction of PBLG-*b*-PEG ($f_{PBLG\text{-}b\text{-}PEG}$) in the polymer mixture was 0.8. Scale bars: 100 nm.

d shows typical multistranded helical structures self-assembled under various experimental conditions. For the detailed morphologies of the helical structures, refer to Figure S4 in the Supporting Information. In addition to rod-like helical structures, toroidal aggregates can also be seen in the SEM images. The formation mechanism of the toroidal structure is also an interesting research subject,[15] and more details regarding the toroids are available in the Supporting Information, Section 5.

Dependence of the Strand Number on the Initial Polymer Concentration

Figure 3a and b show the morphologies of helical aggregates self-assembled at different initial concentrations. As the initial polymer concentration was increased from 0.50 to 1.00 g L^{-1}, superhelices with larger strand numbers were observed. To show the dependence of the strand number on the initial polymer concentration quantitatively, the average number of strands on each superhelical aggregate was measured based on approximately 100 helices. Figure 3e shows the strand number distribution of the superhelices formed from samples with various initial concentrations. The columns represent the length percentage of each type of superhelix, which is the measured length of the superhelical assembly with the same strand number as a percentage of the total length of the self-assembly. The stand number was deduced from the SEM images by considering the geometrical property of the helical structure, which is represented in Figure 2a and d. As shown in Figure 3e, most of the superhelical structures were single stranded (≈69.0%) at an initial concentration of 0.25 g L^{-1}, and the rest of the helices were zero stranded (≈31.0%; the abacus-like structure can be considered a specific case of a helix with a strand number of 0, as discussed below). When the initial concentration was increased to 0.5 g L^{-1}, a few double helices were observed (≈17.6%). Most of the helices still possessed single strands (≈81.3%), and the percentage of zero-strand helices decreased (≈1.1%). At a higher initial concentration of 0.75 g L^{-1}, both double (≈50.7%) and single helices (≈48.5%) became dominant. Triple helices (≈12.2%) mixed with double (≈57.9%) and single helices (≈29.9%) were obtained when the concentration reached 1 g L^{-1}. The dependence of the average strand number on the initial concentration is shown in Figure 3f. The error bars represent the dispersity of the strand number of the superhelices. It clearly reveals that the average strand number increases as the initial polymer concentration was increased. At even higher concentrations the polymers precipitated, which indicated the formation of large aggregates that could net be suspended in the aqueous solution.

Dependence of the Strand Number on the Self-Assembly Temperature

In addition to the initial concentration, we examined the influence of the self-assembly temperature (*T*) on the strand number of the superhelical structures. On comparing Figure 3a and c, we observed superhelices with more strands at higher temperatures (for more details, see the SEM images of the superhelical structures formed at temperatures of 20–50 °C in the Supporting Information, Figure S2 e–h). The distributions of multistranded superhelices were examined at various temperatures. As shown in Figure 3g, most of the superhelical structures were single helices (≈77.4%) at 20 °C. The percentage of zero- and double-stranded helices was approximately 16.8 and 5.8%, respectively. When the temperature was increased to 30 °C, the percentage of single helices decreased to about 44.8% and the percentage of double helices increased to around 46.0%. At higher temperatures of 40 and 50 °C, most of the superhelical structures became double helices, and triple helices were also obtained. The relationship between the average strand number and self-assembly temperature is shown in Figure 3h, which reveals an increase in average strand number with temperature.

As reported in our previous work,[11] the morphology of the helical structure was sensitive to temperature and exhibited switchable characteristics before being frozen by dialysis. We prepared assemblies by adding water (15.0 vol% of the initial solvent) to the polymer solution (initial solvent: THF/DMF, 3:7

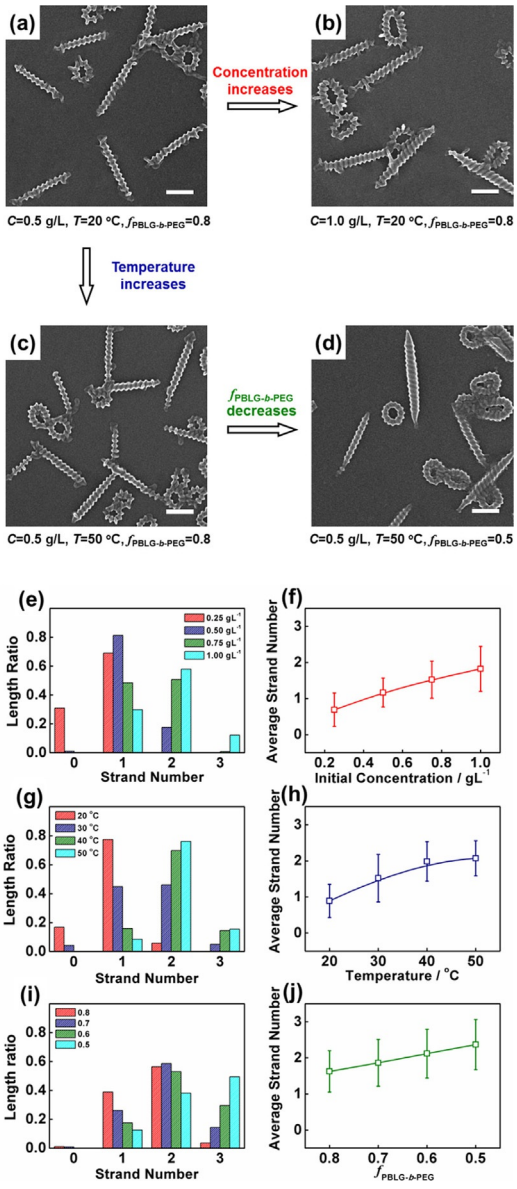

Figure 3. SEM images of helical aggregates self-assembled from $PBLG_{20000}$-*b*-PEG_{5000}/$PBLG_{528000}$ under various experimental conditions: a) $C=0.5\ g\,L^{-1}$, $T=20\,^{\circ}C$, $f_{PBLG\text{-}b\text{-}PEG}=0.8$; b) $C=1.0\ g\,L^{-1}$, $T=20\,^{\circ}C$, $f_{PBLG\text{-}b\text{-}PEG}=0.8$; c) $C=0.5\ g\,L^{-1}$, $T=50\,^{\circ}C$, $f_{PBLG\text{-}b\text{-}PEG}=0.8$; and d) $C=0.5\ g\,L^{-1}$, $T=50\,^{\circ}C$, $f_{PBLG\text{-}b\text{-}PEG}=0.5$. Scale bars: 400 nm. Strand number distribution of superhelices self-assembled under various experimental conditions: e) initial concentration, g) temperature, and i) weight fraction of PBLG-*b*-PEG ($f_{PBLG\text{-}b\text{-}PEG}$). Relationship between the average strand number and various experimental conditions: f) initial concentration, h) temperature, and j) weight fraction of PBLG-*b*-PEG ($f_{PBLG\text{-}b\text{-}PEG}$).

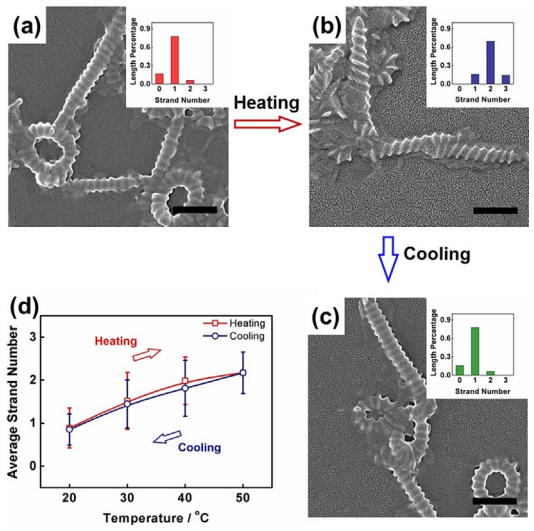

Figure 4. Temperature-induced reversible transition of multistranded superhelices: a) helical structures self-assembled at 20 °C; b) multistranded helices obtained by heating the 20 °C solution to 50 °C; and c) superhelices obtained by cooling the 50 °C solution to 20 °C. Insets: The corresponding strand number distribution. d) Dependence of the average strand number on temperature. At each temperature, the solution was equilibrated for at least 10 h. The added water content in the initial solvent was 15.0 vol%. The initial polymer concentration was $0.5\ g\,L^{-1}$ and the weight fraction of PBLG-*b*-PEG ($f_{PBLG\text{-}b\text{-}PEG}$) in the polymer mixture was 0.8. To obtain clear images, we froze the equilibrated samples by using dialysis at each observation point. Scale bars: 400 nm.

v/v) at 20 °C. Before dialysis against water to freeze the nanostructures, we heated the solution to 50 °C and then cooled it to 20 °C to investigate the effect of temperature on the strand number of the helices (the annealing time at each temperature was no less than 10 h). Figure 4a–c shows the SEM images of the helical structure in this process, and Figure 4, insets, represent the strand number distributions. As shown in Figure 4a, most of the self-assembled structures were single helices at 20 °C (≈77.4%). After annealing at 50 °C for more than 10 h (Figure 4b), most of the helices were converted to double helices (≈69.7%). When the samples were cooled to 20 °C (Figure 4c) after annealing at 50 °C, the helices were converted back to single helices and the strand number distribution was nearly the same as the distribution before annealing. The data on the average strand number as a function of annealing temperature are shown in Figure 4d. The strand number of the superhelical structure is reversible based on the temperature. Before the organic solvent was totally removed, the packing of the PBLG blocks on the homopolymer bundle was not frozen and could reorganize according to the temperature change to reach thermal equilibrium. These observations clearly demonstrate that the multistranded superhelices have switchable features. Moreover, it was noted that the multistranded helical structures can be equilibrated in a short time after the addition of water but before being frozen by dialysis. The annealing time had a negligible effect on the strand number of the self-assembled helices (Figure S6).

Dependence of the Strand Number on the Block Copolymer Fraction in the Mixture

The weight fraction of PBLG-*b*-PEG ($f_{PBLG\text{-}b\text{-}PEG}$) also influences the strand number of the superhelices. The helical aggregates shown in Figure 3d were self-assembled from polymer mixtures with a lower $f_{PBLG\text{-}b\text{-}PEG}$ value, and images of the multistranded helical structures self-assembled with various weight fractions of PBLG-*b*-PEG are shown in the Supporting Information, Figure S4 i–l. Notably, the diameter of the helices in-

creased as the PBLG-*b*-PEG weight fraction was decreased. From the strand number distributions (Figure 3i), we can see that the polymer mixtures tended to form helical structures with more strands at lower weight fractions of PBLG-*b*-PEG. Figure 3j shows the dependence of the average strand number on $f_{PBLG\text{-}b\text{-}PEG}$ and reveals that the average strand number increased as the was $f_{PBLG\text{-}b\text{-}PEG}$ decreased, which is similar to the results for increased initial polymer concentration.

Geometric Parameters of the Multistranded Superhelical Structures

To understand the multistranded features of the superhelices, we first stated the relationship between the strand number and the basic geometric parameters of the helix. Figure 5a and b shows typical schematic illustrations of double helices. There are four basic geometric parameters, *l*, *p*, *d*, and α, which represent the lead, pitch, diameter, and helical angle, respectively.

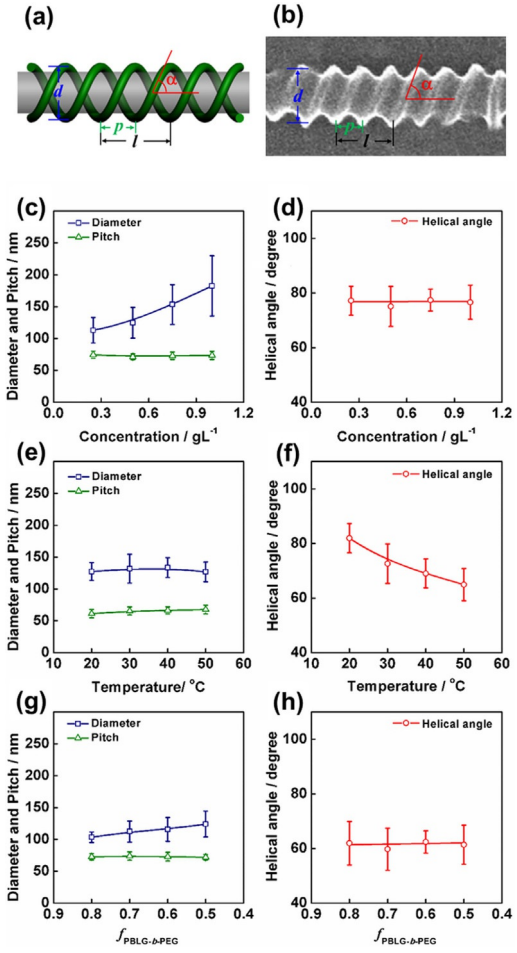

Figure 5. a) Schematic illustration and b) SEM image of the basic geometric parameters of the helical structure. c) Dependence of the diameter (*d*) and pitch (*p*) on the initial concentration. d) Dependence of the helical angle (α) on the initial concentration. e) Dependence of the diameter (*d*) and pitch (*p*) on the self-assembly temperature. f) Dependence of the helical angle (α) on the self-assembly temperature. g) Dependence of the diameter (*d*) and pitch (*p*) on the weight fraction of PBLG-*b*-PEG ($f_{PBLG\text{-}b\text{-}PEG}$). h) Dependence of the helical angle (α) on the weight fraction of PBLG-*b*-PEG ($f_{PBLG\text{-}b\text{-}PEG}$).

The lead (*l*) is the axial advance of a helix in one complete turn (360°). The pitch (*p*) is the axial distance between adjacent threads on a helix. For a single helix, the lead and pitch are the same. For a multistranded helix, the lead is equal to the pitch multiplied by the number of strands ($l = np$, *n* represents the number of strands, details are given in the Supporting Information, Figure S3). The helical angle (α) is the angle between the axis and the tangent line at any point on the helix. The relationship between the strand number and these parameters on a helix follows Equation (1):[16]

$$l = np = \pi d \cot \alpha \quad (1)$$

When the helical angle was 90°, the aggregate appeared to have an abacus-like structure, which was reported in our previous work, and the strand number was calculated to be 0 according to Equation (1).[9b] Therefore, the abacus-like structure can be considered a specific case of a helix with a strand number of 0.

Based on the geometric principle discussed above, we then analyzed the dependence of the three basic geometric parameters, that is, pitch (*p*), diameter (*d*), and helical angle (α), on the initial concentration (*C*) to explain the observation of multistranded superhelices at higher initial concentrations. Figure 5c shows the dependence of the pitch and diameter on the initial concentration. Figure 5d represents the variation in helical angle as a function of the initial concentration. The average diameter was calculated based on more than 50 helical assemblies. Every point of the pitch and helical angle was taken into statistical analysis with 50 points measured from SEM images. Figure 5c shows that the average diameter of the helices increased from 112 to 182 nm as the initial concentration was increased from 0.25 to 1 g L^{-1}. At the same time, the average pitch remained at approximately 125 nm and the helical angle remained at about 76.6°. At higher initial polymer concentrations, more aggregates could be formed in the system, which led to a larger interface between hydrophilic and hydrophobic domains and less stable aggregates with higher interface energy. To reduce the interface energy, larger assemblies with larger aggregation numbers were formed at higher initial concentrations.[17] Therefore, helices with larger diameters could be formed. According to Equation (1), the increase in diameter (*d*) led to an increased strand number (*n*). As a result, helices with a larger numbers of strands could be obtained at higher initial concentrations.

Moreover, the dependence of the pitch (*p*), diameter (*d*), and helical angle (α) on the self-assembly temperature (*T*) were examined to clarify the temperature-dependent variation in the strand number. As shown in Figure 5e, the average pitch and helical diameter remained almost constant as the temperature was increased. Figure 5f represents the dependence of the average helical angle on the self-assembly temperature. At 20 °C, the average helical angle of the helices was approximately 81.9°, and when the temperature was increased to 50 °C, the average helical angle decreased to about 64.9°. As revealed in a previous work,[11] the packing mode of pendant phenyl groups in the side chains of the PBLG blocks are re-

sponsible for the helical angle of the screwed helix. Higher temperatures induce arrangements of the phenyl side groups with higher chirality, which result in a smaller helical angle in the superhelices. According to Equation (1), the decrease in helical angle (α) leads to an increased strand number (n). Thus, helices with more strands can be obtained at higher temperatures.

Similar to the effect of the initial concentration, the average helical diameter increased linearly as the weight fraction of PBLG-*b*-PEG ($f_{PBLG\text{-}b\text{-}PEG}$) was decreased (Figure 5g). As shown in Figure 5g and h, the average pitch and helical angle remained constant with the decrease in $f_{PBLG\text{-}b\text{-}PEG}$. In self-assembled systems, the amphiphilic diblock copolymers can be considered as a dispersant to stabilize the template bundle, which consists of hydrophobic PBLG homopolymers. Decreasing the weight fraction of PBLG-*b*-PEG ($f_{PBLG\text{-}b\text{-}PEG}$) in the polymer mixtures results in the formation of aggregates with a larger aggregation number to reduce the interface area. Therefore, helices with larger diameters can be obtained with lower $f_{PBLG\text{-}b\text{-}PEG}$ values. The increase in diameter (d) results in an increased strand number (n) according to Equation (1). Consequently, the polymer mixtures tend to form helical structures with larger strand numbers at lower weight fractions of PBLG-*b*-PEG.

From the above observations, we can see that the helical pitch always remains constant, independent of the initial concentration, the self-assembly temperature, and the weight fraction of the block copolymers. To understand why the helical pitch remained unchanged, we examined the helical pitch of superhelices self-assembled from mixtures that contained PBLG-*b*-PEG with different PBLG lengths. The average pitch (p) of the helices is plotted as a function of the PBLG block molecular weight in Figure 6. In the self-assembled helices, the homopolymers formed a template bundle and the strands were formed by the screwed arrangement of the block copolymers. Moreover, because the block copolymers form the screwed strands on the homopolymer template bundle to prevent exposure of the hydrophobic homopolymer, the pitch (p) of the helices was determined by the length of the PBLG blocks. Therefore, an increase in the molecular weight of the PBLG blocks led to increased strand widths. In this case, except for the molecular weight of the PBLG blocks, the concentration, temperature, and weight fraction of block copolymers hardly influenced the pitch (p) of the helices.

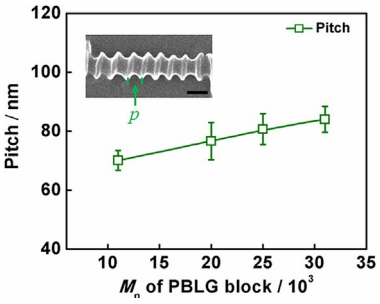

Figure 6. Dependence of the pitch (p) on the molecular weight of the PBLG block. The self-assemblies were prepared at 50 °C. The initial concentration was 0.5 g L^{-1} and the weight fraction of PBLG-*b*-PEG ($f_{PBLG\text{-}b\text{-}PEG}$) was 0.8.

Dislocations in the Multistranded Superhelical Structures

As discussed above, the strand number of the helix is determined by geometric parameters, such as the pitch (p), diameter (d), and helical angle (α). In general, the number of strands on an integrated helix should be an integer. However, the co-influences of the geometric parameters do not always result in an integer strand number. In this case, dislocations appear in the helical structure. Through such a dislocation, the helical strand number can change within a single aggregate. Figure 7 shows the SEM and TEM images of self-assembled helical structures with dislocations marked by red arrows. Figure 7a shows the transition of a single helix to an abacus structure (a specific case for a strand number of zero) at the dislocation site. Additionally, the strand numbers on the helix change from 2 to 1 and 3 to 2 through dislocations (Figure 7b–d). As shown in Figure 7c and d, the helical structures have spindle-like morphologies, which means that the diameter of the helix be-

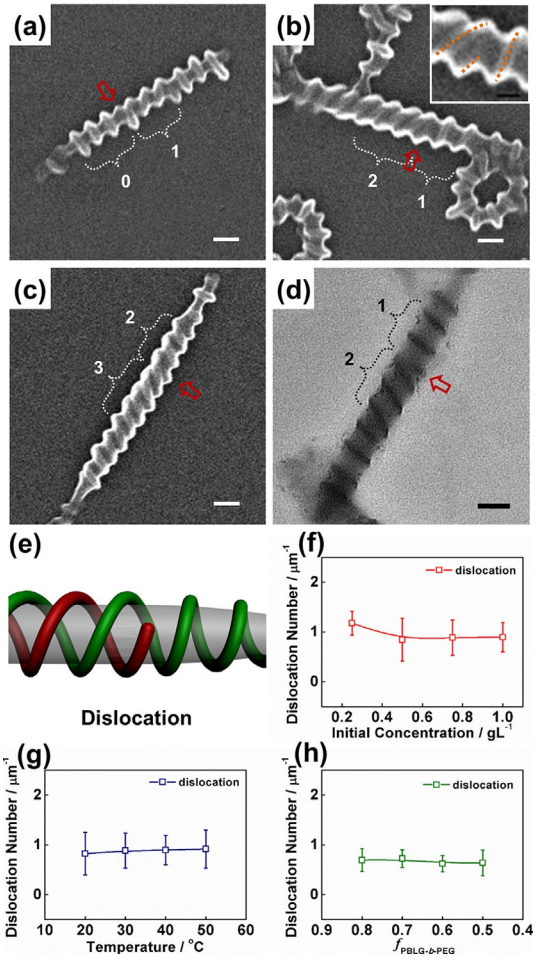

Figure 7. a)–c) SEM and d) TEM images of helical aggregates self-assembled from $PBLG_{20000}$-*b*-PEG_{5000}/PS_{528000}. The red arrows in the images mark the position of dislocations. The numbers in the images represent the strand numbers of the helical structures. Inset: A magnified dislocation. Scale bars: 100 nm (a–d) and 50 nm (inset). e) Schematic illustration of a dislocation in a helical structure. Dislocation number per unit length as a function of f) initial concentration, g) temperature, and h) weight fraction of PBLG-*b*-PEG ($f_{PBLG\text{-}b\text{-}PEG}$).

comes smaller close to the end of each helix. In this case, dislocations appear close to the end of each helix due to the change in diameter.

The dislocations in the superhelices are an interesting finding of this work. The existence of defects, such as dislocations, is an important natural geometrical phenomenon in striped patterns.[18] The distributions and dynamics of defect features in two-dimensional (2D) striped patterns have been studied by both simulation and experimental methods.[19] When striped patterns appear on spherical or curved surfaces, the curvature of the substrates imposes a topological requirement on the equilibrium structure with defects, which includes dislocations, $+1$ disclinations, and $\pm 1/2$ disclinations.[20] These defects in the system can minimize the free energy and equilibrate the structure. The multistranded helix formed in our system is a specific case of strands confined on a cylindrical substrate. Compared with the appearance of defects on planar and spherical surfaces, the defects in multistranded helices have new features. From the schematic illustration of the dislocation structure in the helix (Figure 7e), we can observe that the helix changes from double stranded to single stranded at the dislocation. Additionally, only dislocations are formed in the present case. This observation is in good agreement with the theoretical predictions made by Xing.[21] Dislocation is produced in the helical strands on cylinder substrates on which the strand number of helices is changed, so that the system can maintain the state with lowest free energy. This prediction is, for the first time, verified by our experiments. Figure 7f shows the dependence of the average dislocation number on the initial concentration. The average dislocation number represents the dislocation number per unit length of the helical structures. As observed, the average dislocation number of superhelices obtained at 0.25 g L^{-1} was larger because their average length was shorter than those formed at higher concentrations and the dislocations usually appear near the end of each helix. As the initial concentration was increased from 0.50 to 1 g L^{-1}, the average dislocation number remained constant. Additionally, changes in the temperature or PBLG-*b*-PEG weight fraction hardly influenced the average dislocation number (Figure 7g and h). We also examined the effect of annealing on dislocation and found that the dislocations were stable. The dislocation number remained almost unchanged after the samples were annealed at various temperatures before being frozen by dialysis. Deduced from the above results, dislocation cannot be eliminated in the self-assembled superhelical system. Due to the topological restriction of the aggregates, dislocation is necessary to support multistranded helical strips on a cylinder substrate.

Formation Mechanism of the Multistranded Superhelical Structures

Based on the above investigation and discussion, the formation mechanism of the multistranded superhelical structure is illustrated in Figure 8. The PBLG-*b*-PEG block copolymers and PBLG homopolymers dissolved well in the initial solution. With the addition of water, the PBLG homopolymers aggregated into fibers first because of the lower critical water content (CWC).[11] When further water was added to the solution, the PBLG-*b*-PEG block copolymers self-assembled on the pre-aggregated PBLG homopolymer fiber-like substrates and formed superhelical shells. Finally, the polymer mixtures self-assembled into superhelical structures with uniform pitch and chirality. The strand number is related to the geometric parameters of the helices. At higher initial concentrations of the polymer solution and lower weight fractions of block copolymers in the mixture, the polymer mixtures tended to form helices with larger diameters and a greater number of strands. At higher temperatures,[11] helices with smaller helical angles and a greater number of strands could be obtained because the packing of pendant phenyl side groups had a higher degree of chirality. Additionally, dislocation appears to support the multistranded helical strips due to topological restriction of the aggregates. The existence of dislocations can minimize the free energy in the system and cause strand number transitions within a single helical aggregate.

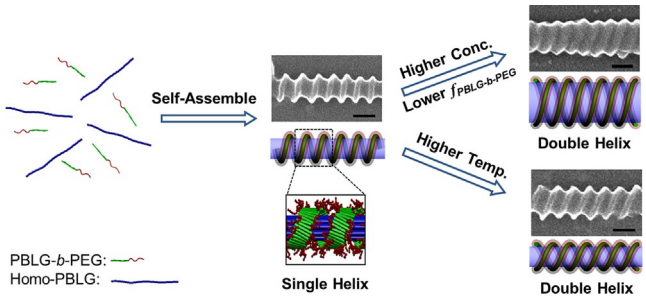

Figure 8. Schematic illustration of the formation of multistranded helices. Scale bars: 100 nm.

As reported in our previous work,[11] right-handed helical structures can also be obtained from the self-assembly of PBLG-*b*-PEG/PBLG mixtures. In the right-handed helical system, multistranded helical structures were also observed. The strand number of the helices increased with increasing initial concentrations, which agrees with the variation of the strand number of superhelices with left-handed chirality (Figure S7).

This work provides a facile self-assembly method to prepare multistranded superhelical structures with controllable characteristics. In our systems, the multistranded helix is a very specific case of strands confined on a cylindrical substrate. On planar and curved surfaces, defects are present in various forms, such as $+1$ disclinations, $\pm 1/2$ disclinations, and dislocations. However, in the multistranded superhelical system, only dislocations were observed. The investigation of multistranded features based on self-assembled superhelices can deepen our understanding of topological dislocations on cylindrical substrates. The superhelices formed in our system have morphologies similar to some natural biological structures. The information gained from this work may provide guidance for revealing the underlying formation mechanism of multistranded helical structures in biological systems in nature. The application of self-assembled multistranded helices as biomimetic particles can help to understand the function of microstructures in biological behavior.

Conclusion

In summary, PBLG-*b*-PEG rod–coil block copolymers and PBLG homopolymers can self-assemble into hierarchical superhelical structures with multiple strands. The strand number of the superhelices can be manipulated through the experimental conditions, such as the initial concentration, self-assembly temperature, and weight fraction of the block copolymers. Higher initial polymer concentrations or lower weight fractions of the block copolymers induce the formation of helices with larger diameters and higher strand numbers. The helices prepared at higher temperatures possess smaller helical angles, which lead to higher strand numbers. Dislocations, an important topological structure in striped patterns, were found in the helical structures. The strand number transition within a single helical aggregate was realized at the dislocations. Finally, a possible mechanism was proposed to illustrate how the initial concentration, temperature, and block copolymer weight fraction influence the multistranded features of the self-assembled superhelical structures. This work provides guidance for the fabrication of superhelical structures with tunable strands.

Experimental Section

Materials

α-Methoxy-ω-amino poly(ethylene glycol) (mPEG-NH_2, $M_n = 5000$) was purchased from Sigma–Aldrich. The mPEG-NH_2 macroinitiator was dried by dissolving it in toluene and then removing the toluene under high vacuum before use. Analytical-grade hexane and 1,4-dioxane were heated at reflux and distilled over sodium immediately before use. Acetic ether was heated at reflux and distilled over CaH_2. Dialysis bags (Membra-cel, 3500 molecular-weight cutoff) were provided by Serva Electrophoresis. All other reagents were purchased from Adamas-beta and used as received. Deionized water (resistance 18.2 MΩ cm) was obtained by using a Millipore Super-Q Plus Water System.

Synthesis of PBLG Homopolymer

γ-Benzyl-L-glutamate-*N*-carboxyanhydride (BLG-NCA) was synthesized according to a previously reported method.[22] PBLG was obtained by ring-opening polymerization of BLG-NCA, which was initiated by using triethylamine with 1,4-dioxane as the solvent. The reaction was performed in a flame-dried reaction bottle under a dry nitrogen atmosphere at 15 °C. After 3 d, the viscous reaction mixture was poured into a large volume of anhydrous ethanol. The precipitated product was dried under vacuum and then purified twice by repeated precipitation from solution in chloroform into a large volume of anhydrous methanol. Gel permeation chromatography (GPC; PL-GPC, Varian) with DMF as the eluent showed that the number-average molecular weight of the PBLG homopolymer was 528000.

Synthesis of PBLG-*b*-PEG Block Copolymer

PBLG-*b*-PEG block copolymers were synthesized by ring-opening polymerization of BLG-NCA in anhydrous 1,4-dioxane, which was initiated by the mPEG-NH_2 macroinitiator as discussed in our previous work.[23] The reaction was performed in a flame-dried reaction bottle under a dry nitrogen atmosphere for 3 d at 15 °C. At the end of the polymerization, the viscous reaction mixture was poured into a large volume of anhydrous ethanol. The precipitated product was filtered and then dried under vacuum. The molecular weight of the block copolymers varied from 12100 to 32000, and the distributions of PBLG-*b*-PEG ranged from 1.13 to 1.26. Detailed results from the polymer characterizations are shown in Table S1 in the Supporting Information.

Preparation of Helical Structures

Inspired by the strategy of polymer multicomponent self-assembly,[24] we prepared superhelical structures from a solution of PBLG-*b*-PEG/PBLG mixtures. First, PBLG-*b*-PEG block copolymers and PBLG homopolymers were dissolved in a mixture of tetrahydrofuran (THF) and *N*,*N*′-dimethylformamide (DMF; 3:7, v/v) with stirring. Then, the block copolymer and homopolymer solutions were mixed at the designated volume ratio (e.g., for a ratio of 4:1, PBLG-*b*-PEG block copolymer solution (3.2 mL) and PBLG homopolymer solution (0.8 mL) were mixed). To prepare the self-assemblies, deionized water (1.5 mL) was added to the initial polymer solution (4 mL) with vigorous stirring. After the addition of water, the colorless solution developed a blue tint, which indicated the formation of self-assembled structures.[9b] After stabilization for at least 1 h, the solution was dialyzed against deionized water for 3 d to ensure that all the organic solvents were removed. The superhelical aggregates were stable in water after dialysis and the storage temperature had a negligible effect on the structures of the self-assembled aggregates. After storing the solution at a different temperature for more than three months, no morphological changes were observed.

The effect of concentration was evaluated by using initial polymer concentrations of 0.25, 0.50, 0.75, and 1.00 g L^{-1}. The self-assembly temperature was fixed at 20 °C, and the weight fraction of PBLG-*b*-PEG ($f_{PBLG\text{-}b\text{-}PEG}$) in the polymer mixtures was 0.8. All of the experiments, including the addition of water and dialysis, were performed at a constant temperature. The effect of the self-assembly temperature was evaluated at temperatures of 20, 30, 40, and 50 °C. The polymer concentration was fixed at 0.5 g L^{-1} and the weight fraction of PBLG-*b*-PEG ($f_{PBLG\text{-}b\text{-}PEG}$) was 0.8. The polymer solutions and water used for the self-assembly procedures were stored at the corresponding temperature for at least 12 h, and all of the experimental procedures were performed at the relevant temperature. To investigate the effect of the block copolymer weight fraction, the block copolymer and homopolymer solutions were mixed with a series of PBLG-*b*-PEG weight fractions of 0.8, 0.7, 0.6, and 0.5. The polymer concentration was 0.5 g L^{-1} and the self-assembly temperature was fixed at 50 °C.

Scanning Electron Microscopy (SEM)

The morphology of the aggregates was observed by using field-emission SEM (S4800, HITACHI) at an accelerating voltage of 15 kV. The samples were prepared by placing drops of solution on a copper grid coated with carbon film, which were then dried at RT. Before the observations, the samples were sputtered with gold.

Transmission Electron Microscopy (TEM)

The morphology of the aggregates were examined by using field-emission TEM (JEM-2100F, JEOL) at an accelerating voltage of 200 kV. Drops of solution were placed on a copper grid coated with carbon film and then dried at RT. For the ultramicrotomed sample, an aqueous solution of superhelices was freeze-dried and the powdered sample was then embedded in epoxy resin and ul-

tramicrotomed. The thickness of the ultramicrotomed sample was approximately 40 nm.

Atomic Force Microscopy (AFM)

AFM measurements were performed at RT in air by using an XE-100 (Park Systems) instrument in noncontact mode. The samples were prepared by placing drops of solution on a silicon wafer surface and allowing the drops to dry in air.

Cryo-TEM

Cryo-TEM samples were prepared in a controlled-environment vitrification system (CEVS). One drop of solution was placed on a copper grid coated with carbon film and excess solution was blotted with a piece of filter paper before the grid was quickly dipped into liquid ethane, which was cooled with liquid nitrogen. The vitrified samples were then stored in liquid nitrogen until they were transferred to a cryogenic sample holder (Gatan 626) and examined by using a JEM-2200FS TEM instrument at an accelerating voltage of 200 kV and at approximately −174 °C.

Acknowledgements

This work was supported by the National Natural Science Foundation of China (21234002, 51303055, 21474029, and 51573049) and the National Basic Research Program of China (2012CB933600). Support from Project of Shanghai Municipality (14DZ2261205) is also appreciated.

Keywords: helical structures · multiple strands · peptides · self-assembly · superhelices

[1] a) S. Zhang, *Nat. Biotechnol.* **2003**, *21*, 1171 – 1178; b) M. A. Meyers, P.-Y. Chen, A. Y.-M. Lin, Y. Seki, *Prog. Mater. Sci.* **2008**, *53*, 1 – 206.
[2] a) A. C. Bloomer, J. N. Champness, G. Bricogne, R. Staden, A. Klug, *Nature* **1978**, *276*, 362 – 368; b) A. Klug, *Philos. Trans. R. Soc. London Ser. B* **1999**, *354*, 531 – 535.
[3] J. D. Watson, G. S. Stent, *The Double Helix : A Personal Account of the Discovery of the Structure of DNA*, Atheneum, New York, **1980**.
[4] a) A. Rich, *Gene* **1993**, *135*, 99 – 109; b) V. N. Soyfer, V. N. Potaman, *Triple-Helical Nucleic Acids*, Springer, New York, **1996**.
[5] a) B. Brodsky, J. A. M. Ramshaw, *Matrix Biol.* **1997**, *15*, 545 – 554; b) J. Engel, H. Bächinger in *Structure, Stability and Folding of the Collagen Triple Helix, Vol. 247*, Springer, Berlin-Heidelberg, **2005**, pp. 7 – 33.
[6] a) R.-M. Ho, Y.-W. Chiang, S.-C. Lin, C.-K. Chen, *Prog. Polym. Sci.* **2011**, *36*, 376 – 453; b) J. Song, Q. Cheng, S. Kopta, R. C. Stevens, *J. Am. Chem. Soc.* **2001**, *123*, 3205 – 3213; c) C.-K. Chen, S.-C. Lin, R.-M. Ho, Y.-W. Chiang, B. Lotz, *Macromolecules* **2010**, *43*, 7752 – 7758; d) J. F. Reuther, D. A. Siriwardane, R. Campos, B. M. Novak, *Macromolecules* **2015**, *48*, 6890 – 6899; e) R.-M. Ho, Y.-W. Chiang, C.-K. Chen, H.-W. Wang, H. Hasegawa, S. Akasaka, E. L. Thomas, C. Burger, B. S. Hsiao, *J. Am. Chem. Soc.* **2009**, *131*, 18533 – 18542; f) Q. Jin, L. Zhang, M. Liu, *Chem. Eur. J.* **2013**, *19*, 9234 – 9241; g) Q. Meng, K. Wang, W. Guo, J. Fang, Z. Wei, X. She, *Small* **2014**, *10*, 3187 – 3193; h) M.-Q. Zhao, Q. Zhang, G.-L. Tian, F. Wei, *Nanoscale* **2014**, *6*, 9339 – 9354; i) Z. Ren, P.-X. Gao, *Nanoscale* **2014**, *6*, 9366 – 9400; j) P. Xing, X. Chu, M. Ma, S. Li, A. Hao, *Chem. Asian J.* **2014**, *9*, 3440 – 3450.
[7] a) O. V. Kulikov, D. A. Siriwardane, J. F. Reuther, G. T. McCandless, H.-J. Sun, Y. Li, S. F. Mahmood, S. S. Sheiko, V. Percec, B. M. Novak, *Macromolecules* **2015**, *48*, 4088 – 4103; b) J. F. Reuther, D. A. Siriwardane, O. V. Kulikov, B. L. Batchelor, R. Campos, B. M. Novak, *Macromolecules* **2015**, *48*, 3207 – 3216.
[8] a) J. Dupont, G. Liu, K. i. Niihara, R. Kimoto, H. Jinnai, *Angew. Chem. Int. Ed.* **2009**, *48*, 6144 – 6147; *Angew. Chem.* **2009**, *121*, 6260 – 6263; b) S. Zhong, H. Cui, Z. Chen, K. L. Wooley, D. J. Pochan, *Soft Matter* **2008**, *4*, 90 – 93.
[9] a) C. Cai, J. Lin, T. Chen, X.-S. Wang, S. Lin, *Chem. Commun.* **2009**, 2709 – 2711; b) C. Cai, Y. Li, J. Lin, L. Wang, S. Lin, X.-S. Wang, T. Jiang, *Angew. Chem. Int. Ed.* **2013**, *52*, 7732 – 7736; *Angew. Chem.* **2013**, *125*, 7886 – 7890.
[10] a) C. Cai, L. Wang, J. Lin, *Chem. Commun.* **2011**, *47*, 11189 – 11203; b) Y. Li, T. Jiang, S. Lin, J. Lin, C. Cai, X. Zhu, *Sci. Rep.* **2015**, *5*, 10137.
[11] C. Cai, J. Lin, X. Zhu, S. Gong, X.-S. Wang, L. Wang, *Macromolecules* **2016**, *49*, 15 – 22.
[12] a) J. Bae, J.-H. Choi, Y.-S. Yoo, N.-K. Oh, B.-S. Kim, M. Lee, *J. Am. Chem. Soc.* **2005**, *127*, 9668 – 9669; b) J. J. Cornelissen, M. Fischer, N. A. Sommerdijk, R. J. Nolte, *Science* **1998**, *280*, 1427 – 1430; c) C. Y. Li, S. Z. D. Cheng, J. G. Jason, F. Bai, J. Z. Zhang, I. K. Mann, F. W. Harris, L.-C. Chien, D. Yan, T. He, *Phys. Rev. Lett.* **1999**, *83*, 4558 – 4561; d) A. E. Rowan, R. J. Nolte, *Angew. Chem. Int. Ed.* **1998**, *37*, 63 – 68; *Angew. Chem.* **1998**, *110*, 65 – 71; e) W. Zou, Y. Yan, J. Fang, Y. Yang, J. Liang, K. Deng, J. Yao, Z. Wei, *J. Am. Chem. Soc.* **2014**, *136*, 578 – 581.
[13] a) V. Percec, C.-H. Ahn, G. Ungar, D. Yeardley, M. Möller, S. Sheiko, *Nature* **1998**, *391*, 161 – 164; b) H. M. Keizer, R. P. Sijbesma, *Chem. Soc. Rev.* **2005**, *34*, 226 – 234; c) A. D. Brown, L. Naves, X. Wang, R. Ghodssi, J. N. Culver, *Biomacromolecules* **2013**, *14*, 3123 – 3129.
[14] B. O'neill, *Elementary Differential Geometry*, Academic Press, Boston, **2006**.
[15] L. Chen, T. Jiang, J. Lin, C. Cai, *Langmuir* **2013**, *29*, 8417 – 8426.
[16] R. C. Juvinall, K. M. Marshek, *Fundamentals of machine component design*, John Wiley&Sons New York, **2006**.
[17] H. Shen, A. Eisenberg, *J. Phys. Chem. B* **1999**, *103*, 9473 – 9487.
[18] C. Bowman, A. Newell, *Rev. Mod. Phys.* **1998**, *70*, 289 – 301.
[19] a) C. Harrison, D. H. Adamson, Z. Cheng, J. M. Sebastian, S. Sethuraman, D. A. Huse, R. A. Register, P. M. Chaikin, *Science* **2000**, *290*, 1558 – 1560; b) S. Ouk Kim, H. H. Solak, M. P. Stoykovich, N. J. Ferrier, J. J. de Pablo, P. F. Nealey, *Nature* **2003**, *424*, 411 – 414; c) V. Mishra, G. H. Fredrickson, E. J. Kramer, *ACS Nano* **2012**, *6*, 2629 – 2641; d) A. Horvat, G. J. A. Sevink, A. V. Zvelindovsky, A. Krekhov, L. Tsarkova, *ACS Nano* **2008**, *2*, 1143 – 1152; e) J.-W. Park, E. L. Thomas, *Macromolecules* **2006**, *39*, 4650 – 4653.
[20] a) T. Chantawansri, A. Bosse, A. Hexemer, H. Ceniceros, C. García-Cervera, E. Kramer, G. Fredrickson, *Phys. Rev. E* **2007**, *75*, 031802; b) D. R. Nelson, *Nano Lett.* **2002**, *2*, 1125 – 1129; c) D. A. Vega, L. R. Gómez, A. D. Pezzutti, F. Pardo, P. M. Chaikin, R. A. Register, *Soft Matter* **2013**, *9*, 9385 – 9392; d) J. F. Li, J. Fan, H. D. Zhang, F. Qiu, P. Tang, Y. L. Yang, *Eur. Phys. J. E* **2006**, *20*, 449 – 457; e) M. Pinna, S. Hiltl, X. Guo, A. Böker, A. V. Zvelindovsky, *ACS Nano* **2010**, *4*, 2845 – 2855.
[21] X. Xing, *J. Stat. Phys.* **2009**, *134*, 487 – 536.
[22] C. Cai, W. Zhu, T. Chen, J. Lin, X. Tian, *J. Polym. Sci. Part A* **2009**, *47*, 5967 – 5978.
[23] a) C. Cai, L. Wang, J. Lin, X. Zhang, *Langmuir* **2012**, *28*, 4515 – 4524; b) Z. Zhuang, C. Cai, T. Jiang, J. Lin, C. Yang, *Polymer* **2014**, *55*, 602 – 610.
[24] a) G. Cambridge, M. J. Gonzalez-Alvarez, G. Guerin, I. Manners, M. A. Winnik, *Macromolecules* **2015**, *48*, 707 – 716; b) H. A. Klok, S. Lecommandoux, *Adv. Mater.* **2001**, *13*, 1217 – 1229; c) J. Zhu, S. Zhang, K. Zhang, X. Wang, J. Mays, K. L. Wooley, D. Pochan, *Nat. Commun.* **2013**, *4*, 2297.

Manuscript received: October 11, 2016
Revised: November 29, 2016
Accepted Article published: November 30, 2016
Final Article published: December 16, 2016